A novel nano-sized red phosphorus decorated borocarbonitride heterojunction with enhanced photocatalytic performance for tetracycline degradation

Yi Wang[a,b], Xing Zhao[a], Lan Wang[c,*], Yu Yang[b], Limin Jiao[a], Zhihao Wu[a], Xuan Gao[a], Sheng Cheng[d], Mingzhang Lin[a,*]

[a] *School of Nuclear Science and Technology, University of Science and Technology of China, Hefei, Anhui 230026, China*

[b] *Reactor Operation and Application Research Sub-Institute, Nuclear Power Institute of China, Chengdu, Sichuan 610041, China*

[c] *School of Materials, Sun Yat-sen University, Guangzhou, Guangdong 510275, China*

[d] *Instrumental Analysis Center, Hefei University of Technology, Hefei, Anhui 230009, China*

* To whom correspondence should be addressed. E-mail: wanglan_only@163.com (L. Wang), gelin@ustc.edu.cn (M. Z. Lin).

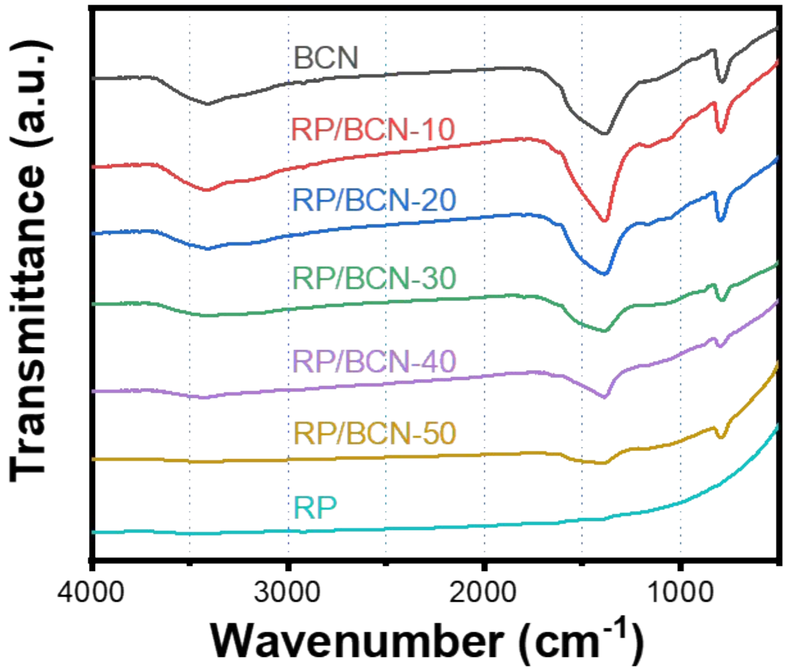

Fig. S1 FT-IR spectra of BCN, RP/BCN, and RP samples.

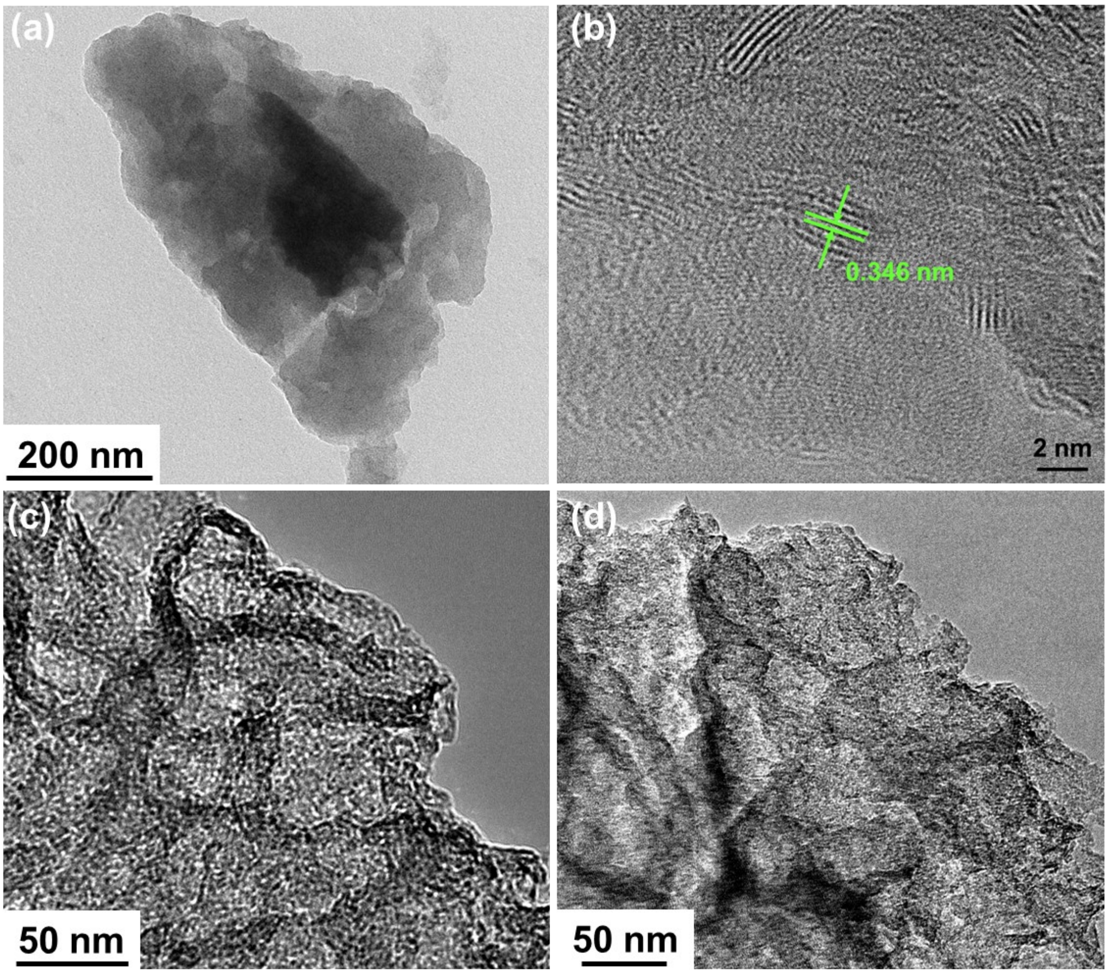

Fig. S2 TEM (**a**) and HR-TEM (**b**) images of BCN. FE-TEM images of BCN (**c**) and RP/BCN-40 (**d**).

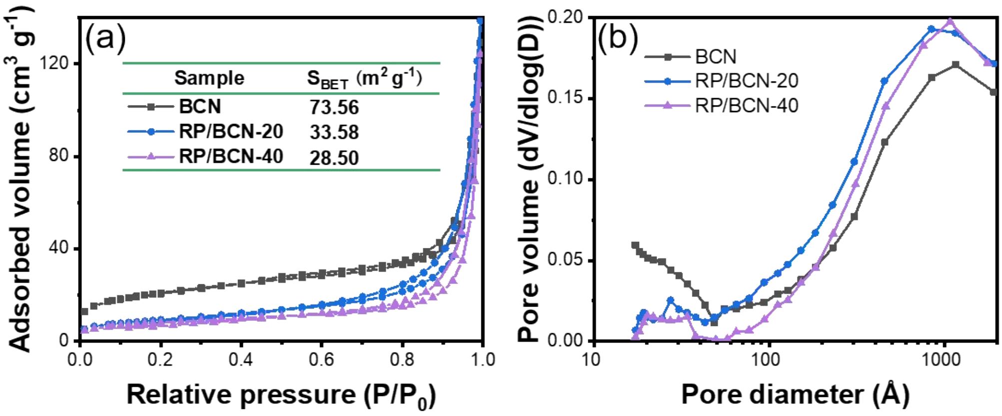

Fig. S3 N_2 adsorption–desorption isotherms (**a**) and BET specific surface area in the inset, and the corresponding BJH pore size distribution (**b**) of BCN, RP/BCN-20 and RP/BCN-40 samples.

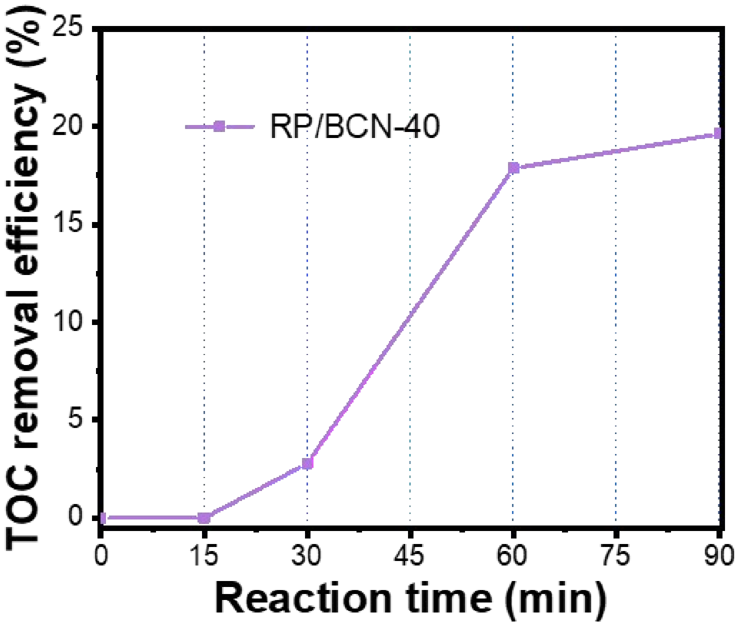

Fig. S4 TOC removal efficiency of TC over RP/BCN-40 under visible exposure.

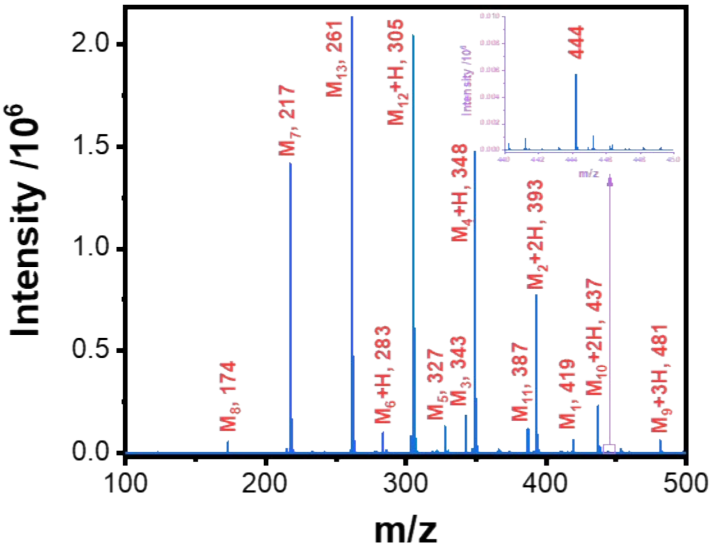

Fig. S5 The UPLC-MS spectra of TC using RP/BCN-40 as the photocatalysts after 120-min exposure.

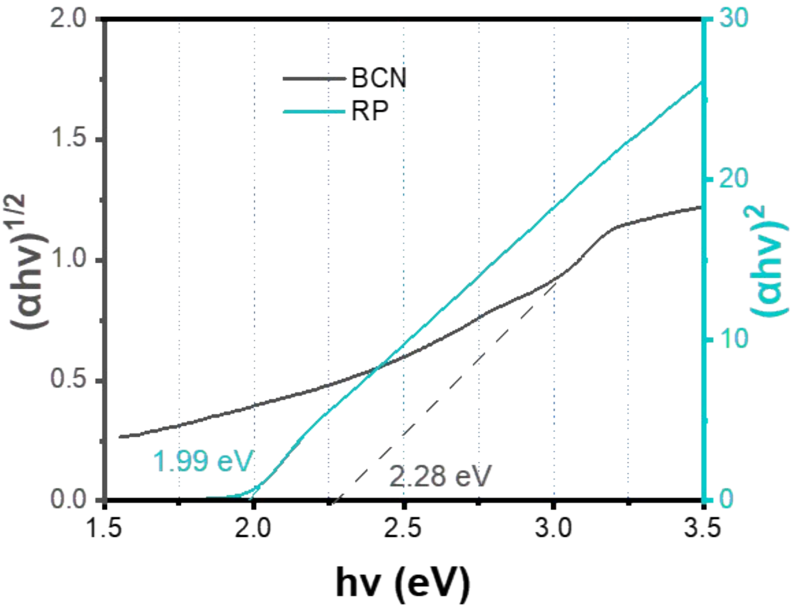

Fig. S6 The band gaps of pure BCN and RP determined by the Tauc plot.

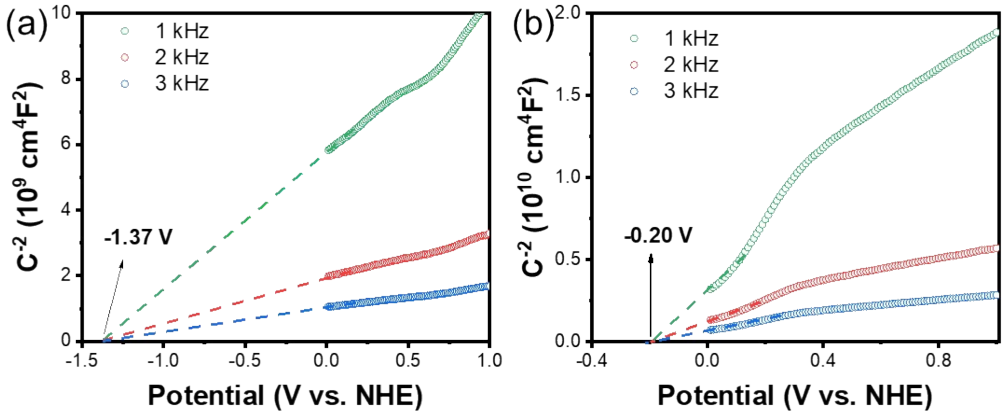

Fig. S7 The electrochemical Mott-Schottky curves for BCN (**a**) and RP (**b**).

Table S1 Elemental analysis from XPS for BCN, RP/BCN, and RP samples.

Sample	B (at%)	C (at%)	N (at%)	P (at%)
BCN	51.59	10.73	37.33	−
RP/BCN-20	50.70	11.04	35.42	2.84
RP/BCN-40	49.51	11.28	34.63	4.59
RP	−	13.34	−	86.66

Table S2 Comparison of TC degradation efficiency and apparent rate constant with previously reported photocatalysts.

Photocatalyst	Reaction condition	Degradation efficiency	Apparent rate constant	References
Ag_3PO_4-PN photocatalyst	TC, 0.03 mg mL^{-1}; catalyst, 2 mg mL^{-1}	85.0%, 120 min	0.0023 min^{-1}	[1]
$LaFeO_3/SnS_2$ hybrid	TC, 0.02 mg mL^{-1}; catalyst, 0.33 mg mL^{-1}	28.8%, 120 min	0.0028 min^{-1}	[2]
BiOI/MIL-125(Ti) composite	TC, 0.02 mg mL^{-1}; catalyst, 0.25 mg mL^{-1}	70.0%, 240 min	0.0048 min^{-1}	[3]
Polyaniline/Perylene diimide organic heterojunction	TC, 0.02 mg mL^{-1}; catalyst, 0.5 mg mL^{-1}	~70%, 120 min	0.0088 min^{-1}	[4]
$AgI/Zn_3V_2O_8$ heterojunction	TC, 0.02 mg mL^{-1}; catalyst, 0.33 mg mL^{-1}	45.4%, 60 min	0.0097 min^{-1}	[5]
Porous hollow cube $ZnFe_2O_4$	TC, 0.04 mg mL^{-1}; catalyst, 0.5 mg mL^{-1}	85.0%, 70 min	0.0118 min^{-1}	[6]
Ag/g-C_3N_4 plasmonic photocatalyst	TC, 0.02 mg mL^{-1}; catalyst, 1.7 mg mL^{-1}	83.0%, 120 min	0.0120 min^{-1}	[7]
Cu_2O–TiO_2–Pal heterojunction	TC, 0.03 mg mL^{-1}; catalyst, 1 mg mL^{-1}	71.5%, 240 min	0.0129 min^{-1}	[8]
$ZnSnO_3$/g-C_3N_4 heterojunction	TC, 0.01 mg mL^{-1}; catalyst, 0.5 mg mL^{-1}	85.0%, 120 min	0.0131 min^{-1}	[9]
Sludge-TiO_2 photocatalysts	TC, 0.005 mg mL^{-1}; catalyst, 0.01 mg mL^{-1}	76.3%, 120 min	0.0142 min^{-1}	[10]
BiOCl microflowers co-modified with oxygen vacancies and Mn^{2+}	TC, 0.02 mg mL^{-1}; catalyst, 1 mg mL^{-1}	~79%, 15 min	0.0146 min^{-1}	[11]
$BiOCl/Bi_2Ti_2O_7$ nanorod	TC, 0.05 mg mL^{-1}; catalyst, 1 mg mL^{-1}	90.0%, 120 min	0.0158 min^{-1}	[12]
Mn-doped $SrTiO_3$ nanocubes	TC, 0.01 mg mL^{-1}; catalyst, 1 mg mL^{-1}	66.7%, 60 min	0.0166 min^{-1}	[13]
γ-In_2Se_3 nanoparticles	TC, 0.02 mg mL^{-1}; catalyst, 1 mg mL^{-1}	91.5%, 120 min	0.0175 min^{-1}	[14]
Cl-doped porous g-C_3N_4 nanosheets	TC, 0.01 mg mL^{-1}; catalyst, 0.5 mg mL^{-1}	92.0%, 120 min	0.0201 min^{-1}	[15]
Carbon dots modified $ZnSnO_3$	TC, 0.02 mg mL^{-1}; catalyst, 1 mg mL^{-1}	81.8%, 60 min	0.0231 min^{-1}	[16]
RP/BCN-40	TC, 0.02 mg mL^{-1}; catalyst, 0.5 mg mL^{-1}	73.8%, 90 min	0.0224 min^{-1}	This work

References

1. Q. Yan, M. Xu, C. Lin, J. Hu, Y. Liu and R. Zhang, Efficient photocatalytic degradation of tetracycline hydrochloride by Ag_3PO_4 under visible-light irradiation, *Environ. Sci. Pollut. R.*, 2016, **23**, 14422-14430.

2. L. Jin, L. Rong, Y. Chen, X. Zhou, X. Ning, Z. Liang, M. Lin, X. Xu, L. Xu and L. Zhang, Rational design of Z-scheme $LaFeO_3/SnS_2$ hybrid with boosted visible light photocatalytic activity towards tetracycline degradation, *Sep. Purif. Technol.*, 2019, **210**, 417-430.

3. W. Jiang, Z. Li, C. Liu, D. Wang, G. Yan, B. Liu and G. Che, Enhanced visible-light-induced photocatalytic degradation of tetracycline using BiOI/MIL-125(Ti) composite photocatalyst, *J. Alloys Compd.*, 2021, **854**, 157166.

4. W. Dai, L. Jiang, J. Wang, Y. Pu, Y. Zhu, Y. Wang and B. Xiao, Efficient and stable photocatalytic degradation of tetracycline wastewater by 3D Polyaniline/Perylene diimide organic heterojunction under visible light irradiation, *Chem. Eng. J.*, 2020, **397**, 125476.

5. J. Luo, X. Ning, L. Zhan and X. Zhou, Facile construction of a fascinating Z-scheme $AgI/Zn_3V_2O_8$ photocatalyst for the photocatalytic degradation of tetracycline under visible light irradiation, *Sep. Purif. Technol.*, 2020, **255**, 117691.

6. Y. Cao, X. Lei, Q. Chen, C. Kang, W. Li and B. Liu, Enhanced photocatalytic degradation of tetracycline hydrochloride by novel porous hollow cube $ZnFe_2O_4$, *J. Photoch. Photobio. A*, 2018, **364**, 794-800.

7. W. Xu, S. Lai, S. C. Pillai, W. Chu, Y. Hu, X. Jiang, M. Fu, X. Wu, F. Li and H. Wang, Visible light photocatalytic degradation of tetracycline with porous Ag/graphite carbon nitride plasmonic composite: degradation pathways and mechanism, *J. Colloid Interface Sci.*, 2020, **574**, 110-121.

8. Y. Shi, Z. Yang, B. Wang, H. An, Z. Chen and H. Cui, Adsorption and photocatalytic degradation of tetracycline hydrochloride using a palygorskite-supported $Cu_2O–TiO_2$ composite, *Appl. Clay Sci.*, 2016, **119**, 311-320.

9. Xiliu, Huang, Feng, Guo, Mingyang, Li, Hongji, Ren and Yu, Hydrothermal synthesis of $ZnSnO_3$ nanoparticles decorated on *g*-C_3N_4 nanosheets for accelerated photocatalytic degradation of tetracycline under the visible-light irradiation, *Sep. Purif. Technol.*, 2020, **230**, 115854.

10. X. Zhu, W. Yuan, M. Lang, G. Zhen, X. Zhang and X. Lu, Novel methods of sewage sludge

utilization for photocatalytic degradation of tetracycline-containing wastewater, *Fuel*, 2019, **252**, 148-156.

11. H. Yu, D. Ge, Y. Liu, Y. Lu, X. Wang, M. Huo and W. Qin, One-pot synthesis of BiOCl microflowers co-modified with Mn and oxygen vacancies for enhanced photocatalytic degradation of tetracycline under visible light, *Sep. Purif. Technol.*, 2020, **251**, 117414.

12. Y. Xu, D. Lin, X. Liu, Y. Luo, H. Xue, B. Huang, Q. Chen and Q. Qian, Electrospun $BiOCl/Bi_2Ti_2O_7$ nanorod heterostructures with enhanced solar light efficiency in the photocatalytic degradation of tetracycline hydrochloride, *ChemCatChem*, 2018, **10**, 2496-2504.

13. G. Wu, P. Li, D. Xu, B. Luo, Y. Hong, W. Shi and C. Liu, Hydrothermal synthesis and visible-light-driven photocatalytic degradation for tetracycline of Mn-doped $SrTiO_3$ nanocubes, *Appl. Surf. Sci.*, 2015, **333**, 39-47.

14. X. Wei, H. Feng, L. Li, J. Gong, K. Jiang, S. Xue and P.K. Chu, Synthesis of tetragonal prismatic γ-In_2Se_3 nanostructures with predominantly {110} facets and photocatalytic degradation of tetracycline, *Appl. Catal. B*, **260**, 118218-118218.

15. F. Guo, M. Li, H. Ren, X. Huang, K. Shu, W. Shi and C. Lu, Facile bottom-up preparation of Cl-doped porous *g*-C_3N_4 nanosheets for enhanced photocatalytic degradation of tetracycline under visible light, *Sep. Purif. Technol.*, 2019, **228**, 115770.

16. F. Guo, X. Huang, Z. Chen, H. Sun and W. Shi, Investigation of visible-light-driven photocatalytic tetracycline degradation via carbon dots modified porous $ZnSnO_3$ cubes: Mechanism and degradation pathway, *Sep. Purif. Technol.*, **253**, 117518.